Supporting Information for:

Chemical Diversity in Lead-Free, Layered Double Perovskites: A Combined Experimental and Computational Approach

Brenda Vargas,[a†] Raúl Torres-Cadena, [a†] Diana T. Reyes-Castillo, [a] Joelis Rodríguez-Hernández,[b] Milan Gembicky,[c] Eduardo Menéndez-Proupin[d] and Diego Solis-Ibarra[a]*

[a] Laboratorio de Fisicoquímica y Reactividad de Superficies (LaFReS), Instituto de Investigaciones en Materiales, Universidad Nacional Autónoma de México, CU, Coyoacán, 04510. Ciudad de México, México. E-mail: diego.solis@unam.mx

[b] Centro de Investigación en Química Aplicada (CIQA)
Blvd. Enrique Reyna Hermosillo, No. 140, Saltillo, Coahuila 25294, México.

[c] Department of Chemistry and Biochemistry, University of California
San Diego, 9500 Gilman Drive, La Jolla, California 92093, United States.

[d] Grupo de Modelación de Materiales, Departamento de Física, Facultad de Ciencias, Universidad de Chile, Las Palmeras, 3425, Ñuñoa 780-0003, Santiago, Chile.

† These authors contributed equally.

* Corresponding author: diego.solis@unam.mx

Table of Contents

Computational Methods

First principle calculations were carried out by using density functional theory (DFT) with a plane-wave basis set and projector augmented wave (PAW)[1] method as implemented in Vienna ab initio simulation package (VASP).[2,3] For relative thermodynamic stability we get the energy of perovskites with the full relaxed structure optimizations using generalized gradient approximation (GGA) formulated by Perdew, Burke, and Ernzehof in the modified form (PBEsol).[4] To perform DFT calculations, the primitive cell was obtained, this primitive cell was achieved using SeeK-path code.[5] An energy cutoff of 330 eV and a 4 x 4 x 2 grid of k-points for Brillouin zone were implemented without symmetric restrictions until the maximum force and energy per atom is < 0.01 eV $Å^{-1}$ and 10 meV, respectively. Our first principle calculations were implemented using the previously reported manganese and copper perovskites ($Cs_4MnSb_2Cl_{12}$ and $Cs_4CuSb_2Cl_{12}$) as the starting point.[6,7] For all the optimizations, we considered spin configurations to those perovskites that contained transition metals with incomplete *d* levels, we considered as a ferromagnetic structure. To obtain the relative thermodynamic stability, all compounds, both products and reagents were optimized as a ferromagnetic configuration. For the relative thermodynamical stability studies, a search for suitable decomposition materials was done at the Materials Project.[8] Detailed information for the decomposition products considering for every material can be found in table S2. When more than one possible decomposition pathway was available, both were calculated and the one with a lower energy was used for analysis.

For the possible stable compounds, as identified with the computational method described above and in the main manuscript (Figure 3), their electronic structure was also calculated. For: $Cs_4FeSb_2Cl_{12}$, $Cs_4CrSb_2Cl_{12}$, $Rb_4CrSb_2Cl_{12}$, $Rb_4MnSb_2Cl_{12}$, $Rb_4CuSb_2Cl_{12}$, $Cs_4CdSb_2Cl_{12}$, $Cs_4MnBi_2Cl_{12}$, $Cs_4FeBi_2Cl_{12}$ and $Cs_4CdBi_2Cl_{12}$, the band structures and density of states (DOS) are shown in Figures S1 and S2. The DOS and band diagrams were obtained with the HSE06 functional,[9,10] starting from structures that were previously relaxed using the same HSE06 functional. Reciprocal coordinates of the *k* points used in the band structure are shown in table S3.

Due the presence of unpaired electrons and partially filled d-shells, it was necessary to consider magnetic configurations, which are: non-magnetic (NM), ferromagnetic (FM) and antiferromagnetic (AFM). Spin configuration that was chosen for AFM is the most stable configuration obtained in previous works.[7,11] For cadmium compounds only the non-magnetic configuration was considered. Being the AFM, the most stable configuration for all compounds with unpair electrons, (table S4).

First, the structures were optimized, using HSE06 functional, without considering the magnetic configuration using the primitive cell, then it was optimized with the desired magnetic configuration, until the maximum force and energy per atom were < 0.01 eV $Å^{-1}$ and 10 meV, respectively. For primitive cells, we implemented a grid of k-points for Brillouin zone of 4 x 4 x 2. For AFM configuration, a 2 x 2 x 1 supercell was created for each compound, for this supercell we used a 2 x 2 x 2 grid of k-points for Brillouin zone, and for both structures, an energy cutoff of 330 eV was used during the structure optimization process.

For the bismuth compounds, the spin orbit coupling was included in the band structure calculation. For manganese and iron compounds, the calculations were performed with an AFM configuration. Table S5 shown the results with non-SOC and SOC calculations for bismuth compounds.

Table S1. Optimized lattice parameters for 25-perovskites with the form $A_4M^{II}M^{III}{}_2Cl_{12}$ using primitive cell using PBEsol functional.

Material			Calculated lattice parameters				
A	**M^{II}**	**M^{III}**	**a = b**	**c**	**α**	**β**	**γ**
Cs	Ti	Sb	7.438	12.849	73.198	106.788	120.064
	V		7.412	12.755	73.109	106.892	120.008
	Cr		7.422	12.743	73.008	106.992	120.048
	Mn		7.438	12.808	73.120	106.871	119.995
	Fe		7.394	12.746	73.104	106.896	119.880
	Co		7.365	12.691	73.208	106.793	120.034
	Cu		7.377	12.814	71.481	108.519	121.179
	Zn		7.422	12.755	73.077	106.923	120.006
	Cd		7.524	12.942	73.106	106.894	120.007
Rb	Ti		7.296	12.682	74.594	105.254	120.664
	V		7.301	12.607	73.181	106.818	120.004
	Cr		7.317	12.574	73.083	106.917	120.009
	Mn		7.327	12.657	73.177	106.823	120.000
	Fe		7.285	12.592	73.108	106.892	119.885
	Co		7.265	12.518	73.132	106.869	120.003
	Cu		7.206	12.443	73.382	106.618	119.869
	Zn		7.323	12.580	73.081	106.919	120.002
	Cd		7.442	12.815	73.090	106.910	120.035
Cs	Ti	Bi	7.45754	12.93239	73.2541	106.7413	119.9877
	V		7.4182	12.87281	73.2557	106.7431	119.9963
	Cr		7.43077	12.87039	73.2242	106.7773	120.0018
	Mn		7.44602	12.9172	73.2475	106.7523	119.9967
	Fe		7.40859	12.8552	73.2454	106.744	119.9945
	Co		7.39183	12.80159	73.229	106.7686	120.0002
	Ni		7.36539	12.76899	73.2273	106.7691	119.988
	Cu		7.36976	12.7667	73.3265	106.6721	119.9353
	Zn		7.43106	12.87007	73.2287	106.7669	119.9938
	Cd		7.53385	13.05844	73.2434	106.7534	119.9988

Table S2. Decomposition pathways for $Cs_4M^{II}Sb_2X_{12}$ and $Rb_4M^{II}Sb_2X_{12}$ and calculated energies considering non-magnetic (NM) and ferromagnetic (FM) configurations for the corresponding transition-metal material.

Perovskite	Decomposition pathway	ΔH_{des} (meV/atom)	
		NM	FM
$Cs_4TiSb_2Cl_{12}$	$CsTiCl_3 + Cs_3Sb_2Cl_9$	–41.658	–25.276
	$TiCl_2 + CsCl + Cs_3Sb_2Cl_9$	–36.446	–13.021
	$CsTiCl_3 + 3\ CsCl + 2\ SbCl_3$	35.623	52.005
	$TiCl_2 + 2\ SbCl_3 + 4\ CsCl$	40.836	64.261
$Cs_4VSb_2Cl_{12}$	$CsVCl_3 + Cs_3Sb_2Cl_9$	–54.079	–9.761
	$VCl_2 + CsCl + Cs_3Sb_2Cl_9$	–47.863	31.421
	$CsVCl_3 + 3\ CsCl + 2\ SbCl_3$	23.023	67.521
	$VCl_2 + 2\ SbCl_3 + 4\ CsCl$	29.418	108.703
$Cs_4CrSb_2Cl_{12}$	$½\ Cs_2CrCl_4 + ½\ CrCl_2 + Cs_3Sb_2Cl_9$	–17.572	5.600
	$CrCl_2 + CsCl + Cs_3Sb_2Cl_9$	–26.987	20.799
	$Cs_2CrCl_4 + 2\ SbCl_3 + 2\ CsCl$	69.123	67.683
	$½\ Cs_2CrCl_4 + ½\ CrCl_2 + 2\ SbCl_3 + 3\ CsCl$	59.709	82.882
	$CrCl_2 + 2\ SbCl_3 + 4\ CsCl$	50.294	98.080
$Cs_4MnSb_2Cl_{12}$	$CsMnCl_3 + Cs_3Sb_2Cl_9$	–23.863	4.712
	$MnCl_2 + CsCl + Cs_3Sb_2Cl_9$	–16.689	24.293
	$CsMnCl_3 + 3\ CsCl + 2\ SbCl_3$	53.418	81.993
	$MnCl_2 + 2\ SbCl_3 + 4\ CsCl$	60.592	101.575
$Cs_4FeSb_2Cl_{12}$	$CsFeCl_3 + Cs_3Sb_2Cl_9$	–21.411	28.886
	$FeCl_2 + CsCl + Cs_3Sb_2Cl_9$	–13.300	36.997
	$CsFeCl_3 + 3\ CsCl + 2\ SbCl_3$	55.870	106.167
	$FeCl_2 + 2\ SbCl_3 + 4\ CsCl$	121.564	114.277
$Cs_4CoSb_2Cl_{12}$	$CsCoCl_3 + Cs_3Sb_2Cl_9$	–7.153	–12.020
	$CoCl_2 + CsCl + Cs_3Sb_2Cl_9$	5.489	17.506
	$CsCoCl_3 + 3\ CsCl + 2\ SbCl_3$	70.127	65.260
	$CoCl_2 + 2\ SbCl_3 + 4\ CsCl$	82.770	94.787
$Cs_4CuSb_2Cl_{12}$	$CsCuCl_3 + Cs_3Sb_2Cl_9$	17.644	12.670
	$CuCl_2 + CsCl + Cs_3Sb_2Cl_9$	28.740	27.350
	$CsCuCl_3 + 3\ CsCl + 2\ SbCl_3$	94.926	89.952
	$CuCl_2 + 2\ SbCl_3 + 4\ CsCl$	106.021	104.641
$Cs_4ZnSb_2Cl_{12}$	$½\ Cs_2ZnCl_4 + ½\ ZnCl_2 + Cs_3Sb_2Cl_9$	–7.191	
	$ZnCl_2 + CsCl + Cs_3Sb_2Cl_9$	10.397	
	$Cs_2ZnCl_4 + 2\ SbCl_3 + 2\ CsCl$	52.503	
	$ZnCl_2 + 2\ SbCl_3 + 4\ CsCl$	87.678	
$Cs_4CdSb_2Cl_{12}$	$CsCdCl_3 + Cs_3Sb_2Cl_9$	1.395	
	$CdCl_2 + CsCl + Cs_3Sb_2Cl_9$	15.376	
	$CsCdCl_3 + 3\ CsCl + 2\ SbCl_3$	78.677	
	$CdCl_2 + 2\ SbCl_3 + 4\ CsCl$	92.658	
$Rb_4CuSb_2Cl_{12}$	$RbCuCl_3 + Rb_3Sb_2Cl_9$	23.137	18.993
	$½\ Rb_2CuCl_4 + ½\ CuCl_2 + Rb_3Sb_2Cl_9$	21.213	20.211
	$CuCl_2 + RbCl + Rb_3Sb_2Cl_9$	27.276	27.275
	$Rb_2CuCl_4 + 2\ SbCl_3 + 2\ RbCl$	60.691	58.466
	$RbCuCl_3 + 2\ SbCl_3 + 3\ RbCl$	68.458	64.314
	$CuCl_2 + 2\ SbCl_3 + 4\ RbCl$	72.596	72.596
$Rb_4TiSb_2Cl_{12}$	$RbTiCl_3 + Rb_3Sb_2Cl_9$	–40.902	–11.880
	$TiCl_2 + RbCl + Rb_3Sb_2Cl_9$	–42.752	–6.955

	$RbTiCl_3 + 2\ SbCl_3 + 3\ RbCl$	4.418	33.440
	$TiCl_2 + 2\ SbCl_3 + 4\ RbCl$	2.568	38.365
$Rb_4VSb_2Cl_{12}$	$RbVCl_3 + Rb_3Sb_2Cl_9$	–53.087	–9.136
	$VCl_2 + RbCl + Rb_3Sb_2Cl_9$	–51.602	26.401
	$RbVCl_3 + 2\ SbCl_3 + 3\ RbCl$	–7.767	26.184
	$VCl_2 + 2\ SbCl_3 + 4\ RbCl$	–6.282	71.722
$Rb_4CrSb_2Cl_{12}$	$½\ Rb_2CrCl_4 + ½\ CrCl_2 + Rb_3Sb_2Cl_9$	–19.998	4.109
	$RbCrCl_3 + Rb_3Sb_2Cl_9$	–67.253	10.841
	$CrCl_2 + RbCl + Rb_3Sb_2Cl_9$	–28.604	15.481
	$Rb_2CrCl_4 + 2\ SbCl_3 + 2\ RbCl$	33.928	38.057
	$RbCrCl_3 + 2\ SbCl_3 + 3\ RbCl$	–21.933	56.161
	$CrCl_2 + 2\ SbCl_3 + 4\ RbCl$	16.716	60.802
$Rb_4MnSb_2Cl_{12}$	$RbMnCl_3 + Rb_3Sb_2Cl_9$	–2.798	8.803
	$Rb_2MnCl_4 + MnCl_2 + Rb_3Sb_2Cl_9$	–7.179	9.852
	$MnCl_2 + RbCl + Rb_3Sb_2Cl_9$	–16.263	17.751
	$Rb_2MnCl_4 + 2\ SbCl_3 + 2\ RbCl$	47.225	47.274
	$RbMnCl_3 + 2\ SbCl_3 + 3\ RbCl$	42.522	54.123
	$MnCl_2 + 2\ SbCl_3 + 4\ RbCl$	29.057	63.071
$Rb_4FeSb_2Cl_{12}$	$RbFeCl_3 + Rb_3Sb_2Cl_9$	–13.848	–10.359
	$FeCl_2 + RbCl + Rb_3Sb_2Cl_9$	–11.172	31.919
	$RbFeCl_3 + 2\ SbCl_3 + 3\ RbCl$	31.472	34.961
	$FeCl_2 + 2\ SbCl_3 + 4\ RbCl$	34.148	77.240
$Rb_4CoSb_2Cl_{12}$	$RbCoCl_3 + Rb_3Sb_2Cl_9$	–0.553	–7.828
	$CoCl_2 + RbCl + Rb_3Sb_2Cl_9$	7.812	15.233
	$½\ Rb_2CoCl_4 + ½\ CoCl_2 + Rb_3Sb_2Cl_9$	25.002	18.391
	$RbCoCl_3 + 2\ SbCl_3 + 3\ RbCl$	44.768	37.492
	$CoCl_2 + 2\ SbCl_3 + 4\ RbCl$	53.133	60.554
	$Rb_2CoCl_4 + 2\ SbCl_3 + 2\ RbCl$	87.613	66.869
$Rb_4CuSb_2Cl_{12}$	$RbCuCl_3 + Rb_3Sb_2Cl_9$	23.137	18.993
	$½\ Rb_2CuCl_4 + ½\ CuCl_2 + Rb_3Sb_2Cl_9$	21.213	20.211
	$CuCl_2 + RbCl + Rb_3Sb_2Cl_9$	27.276	27.275
	$Rb_2CuCl_4 + 2\ SbCl_3 + 2\ RbCl$	60.691	58.466
	$RbCuCl_3 + 2\ SbCl_3 + 3\ RbCl$	68.458	64.314
	$CuCl_2 + 2\ SbCl_3 + 4\ RbCl$	72.596	72.596
$Rb_4ZnSb_2Cl_{12}$	$½\ Rb_2ZnCl_4 + ½\ ZnCl_2 + Rb_3Sb_2Cl_9$	–7.294	
	$ZnCl_2 + RbCl + Rb_3Sb_2Cl_9$	5.587	
	$Rb_2ZnCl_4 + 2\ SbCl_3 + 2\ RbCl$	25.145	
	$ZnCl_2 + 2\ SbCl_3 + 4\ RbCl$	50.907	
$Rb_4CdSb_2Cl_{12}$	$RbCdCl_3 + Rb_3Sb_2Cl_9$	–5.700	
	$CdCl_2 + RbCl + Rb_3Sb_2Cl_9$	5.569	
	$RbCdCl_3 + 2\ SbCl_3 + 3\ RbCl$	39.620	
	$CdCl_2 + 2\ SbCl_3 + 4\ RbCl$	50.890	
$Cs_4TiBi_2Cl_{12}$	$CsTiCl_3 + Cs_3Bi_2Cl_9$	–45.018	–27.011
	$TiCl_2 + CsCl + Cs_3Bi_2Cl_9$	–39.806	–14.755
	$CsTiCl_3 + 2\ BiCl_3 + 3\ CsCl$	29.263	47.270
	$TiCl_2 + 2\ BiCl_3 + 4\ CsCl$	34.475	59.526
$Cs_4VBi_2Cl_{12}$	$CsVCl_3 + Cs_3Bi_2Cl_9$	–56.674	–11.084
	$VCl_2 + CsCl + Cs_3Bi_2Cl_9$	–50.459	30.098
	$CsVCl_3 + 2\ BiCl_3 + 3\ CsCl$	17.607	63.197
	$VCl_2 + 2\ BiCl_3 + 4\ CsCl$	23.822	104.379
$Cs_4CrBi_2Cl_{12}$	$½\ Cs_2CrCl_4 + ½\ CrCl_2 + Cs_3Bi_2Cl_9$	–19.672	–0.915
	$CrCl_2 + CsCl + Cs_3Bi_2Cl_9$	–29.087	14.284
	$Cs_2CrCl_4 + 2\ BiCl_3 + 2\ CsCl$	64.023	58.168

	½ Cs_2CrCl_4 + ½ $CrCl_2$ + 2 $BiCl_3$ + 3 CsCl	54.609	73.366
	$CrCl_2$ + 2 $SbCl_3$ + 4 CsCl	45.194	88.564
$Cs_4MnBi_2Cl_{12}$	$CsMnCl_3$ + $Cs_3Bi_2Cl_9$	–26.572	2.388
	$MnCl_2$ + CsCl + $Cs_3Bi_2Cl_9$	–19.398	21.970
	$CsMnCl_3$ + 2 $BiCl_3$ + 3 CsCl	47.709	76.669
	$MnCl_2$ + 2 $BiCl_3$ + 4 CsCl	54.883	96.251
$Cs_4FeBi_2Cl_{12}$	$CsFeCl_3$ + $Cs_3Bi_2Cl_9$	–25.010	25.822
	$FeCl_2$ + CsCl + $Cs_3Bi_2Cl_9$	–16.899	33.932
	$CsFeCl_3$ + 2 $BiCl_3$ + 3 CsCl	49.271	100.102
	$FeCl_2$ + 2 $BiCl_3$ + 4 CsCl	57.382	108.213
$Cs_4CoBi_2Cl_{12}$	$CsCoCl_3$ + $Cs_3Bi_2Cl_9$	–16.854	–14.941
	$CoCl_2$ + CsCl + $Cs_3Bi_2Cl_9$	–4.211	14.585
	$CsCoCl_3$ + 2 $BiCl_3$ + 3 CsCl	57.427	59.340
	$CoCl_2$ + 2 $BiCl_3$ + 4 CsCl	70.070	88.866
$Cs_4NiBi_2Cl_{12}$	$CsNiCl_3$ + $Cs_3Bi_2Cl_9$	–7.268	–10.297
	$NiCl_2$ + CsCl + $Cs_3Bi_2Cl_9$	9.681	5.105
	$CsNiCl_3$ + 2 $BiCl_3$ + 3 CsCl	67.012	63.983
	$NiCl_2$ + 2 $BiCl_3$ + 4 CsCl	83.961	79.385
$Cs_4CuBi_2Cl_{12}$	$CsCuCl_3$ + $Cs_3Bi_2Cl_9$	2.407	–3.347
	$CuCl_2$ + CsCl + $Cs_3Bi_2Cl_9$	13.503	11.333
	$CsCuCl_3$ + 3 CsCl + 2 $BiCl_3$	76.688	70.934
	$CuCl_2$ + 2 $BiCl_3$ + 4 CsCl	87.784	85.613
$Cs_4ZnBi_2Cl_{12}$	½ Cs_2ZnCl_4 + ½ $ZnCl_2$ + $Cs_3Bi_2Cl_9$	–8.733	
	$ZnCl_2$ + CsCl + $Cs_3Bi_2Cl_9$	8.855	
	Cs_2ZnCl_4 + 2 $BiCl_3$ + 2 CsCl	47.961	
	$ZnCl_2$ + 2 $BiCl_3$ + 4 CsCl	83.136	
$Cs_4CdBi_2Cl_{12}$	$CsCdCl_3$ + $Cs_3Bi_2Cl_9$	0.455	
	$CdCl_2$ + CsCl + $Cs_3Bi_2Cl_9$	14.436	
	$CsCdCl_3$ + 3 CsCl + 2 $BiCl_3$	74.736	
	$CdCl_2$ + 2 $BiCl_3$ + 4 CsCl	88.717	

Table S3. Reciprocal coordinates of *k*-points.

Coordinates			***k*-point**
x	**y**	**z**	
–0.34	0.65	0.00	C_2
–0.50	0.50	0.00	Y_2
0.00	0.00	0.00	Γ
–0.50	0.50	0.50	M_2
-0.30	0.69	0.50	D
0.30	0.30	0.50	D_2
0.00	0.00	0.50	A
0.00	0.50	0.50	L_2
0.00	0.50	0.00	V_2

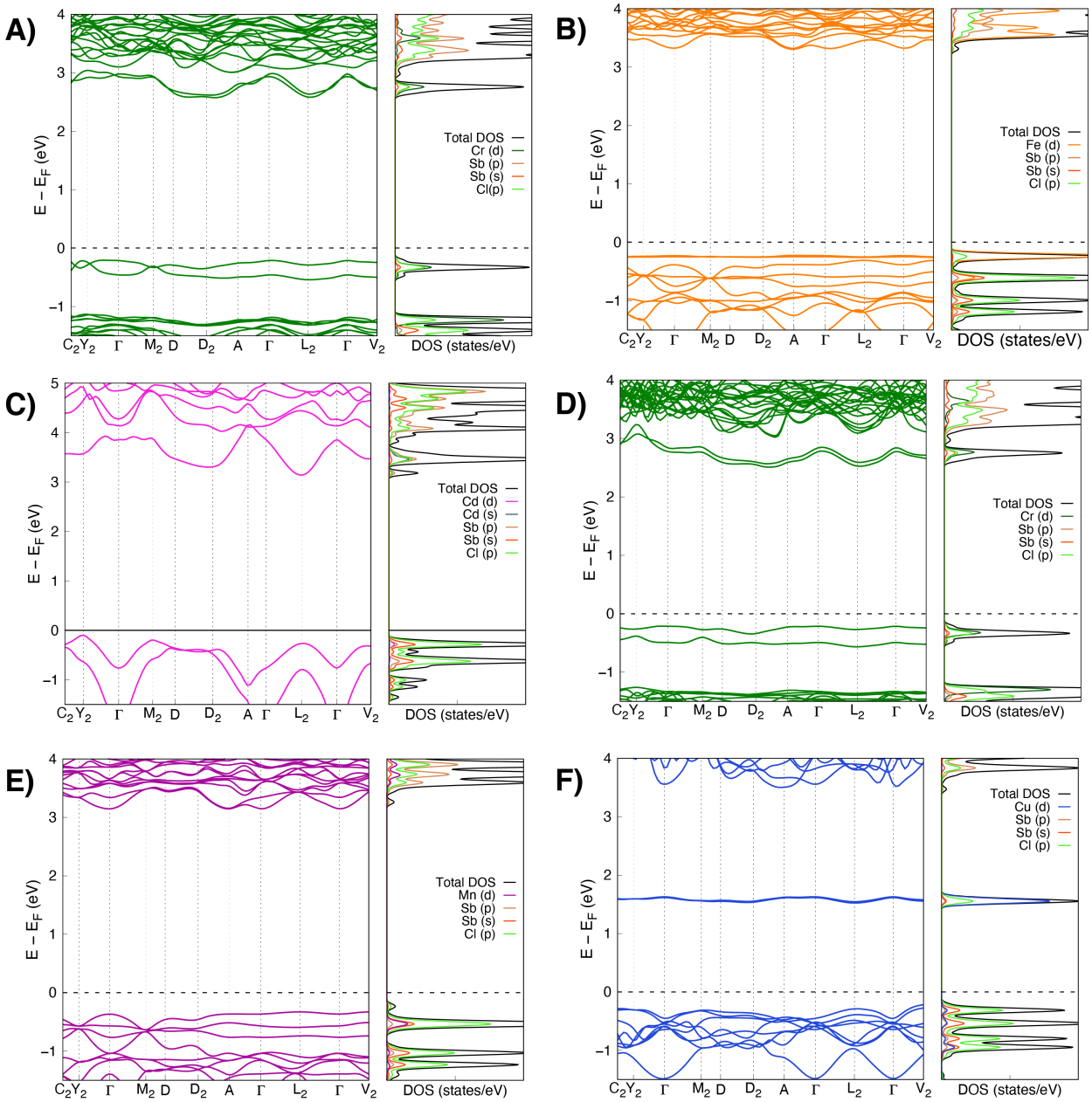

Figure S1. Band structure and density of states of the most stable magnetic configuration obtained for antimony compounds. A) $Cs_4CrSb_2Cl_{12}$, B) $Cs_4FeSb_2Cl_{12}$, C) $Cs_4CdSb_2Cl_{12}$, D) $Rb_4CrSb_2Cl_{12}$, E) $Rb_4MnSb_2Cl_{12}$ and F) $Rb_4CuSb_2Cl_{12}$.

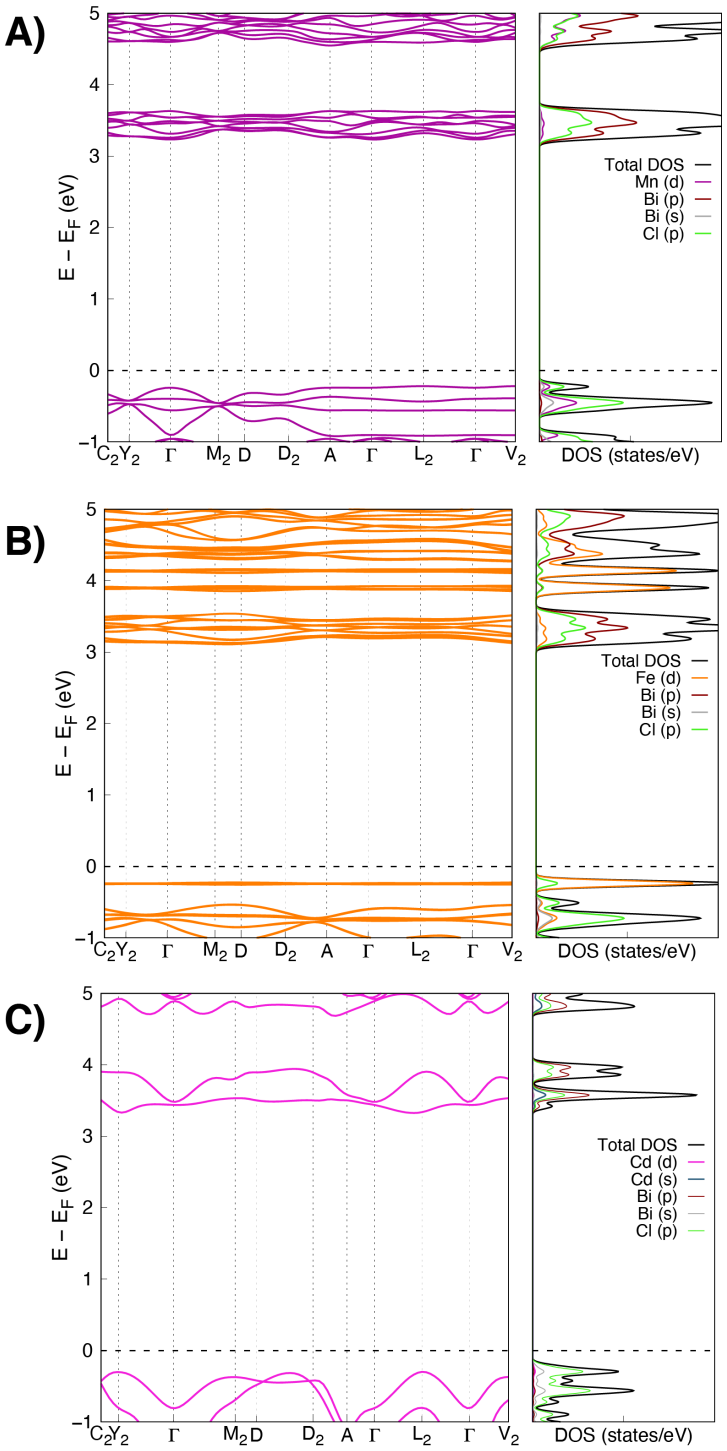

Figure S2. Band structure and density of states of the most stable magnetic configuration obtained for bismuth compounds including the spin orbit coupling. A) $Cs_4FeBi_2Cl_{12}$, B) $Cs_4MnBi_2Cl_{12}$, and C) $Cs_4CdBi_2Cl_{12}$.

Table S4. Band gap (eV) and relative energy per atom (meV/atom) of all magnetic configurations for the perovskites $Cs_4M^{II}Sb_2Cl_{12}$, $Rb_4M^{II}Sb_2Cl_{12}$ and $Cs_4M^{II}Bi_2Cl_{12}$.

Material			Magnetic configuration	Relative energy per atom (meV/atom)
A^+	M^{II}	M^{III}		
Cs	Sb	Cr	NM	0
			FM	–161.153
			AFM	–161.269
		Fe	NM	0
			FM	–107.739
			AFM	–111.081
		Cd	-	-
Rb		Cr	NM	0
			FM	–156.549
			AFM	–156.577
		Mn	NM	0
			FM	–243.111
			AFM	–243.432
		Cu	NM	0
			FM	–24.856
			AFM	–25.741
Material			Magnetic configuration	Relative energy per atom (meV/atom)
A^+	M^{II}	M^{III}		
Cs	Bi	Fe	NM	0
			FM	–108.789
			AFM	–109.702
		Mn	NM	0
			FM	–251.940
			AFM	–253.343
		Cd	-	-

Table S5. Band gap (eV) for the perovskites $Cs_4M^{II}Sb_2Cl_{12}$, $Rb_4M^{II}Sb_2Cl_{12}$ and $Cs_4M^{II}Bi_2Cl_{12}$. For bismuth compounds, it shown the non-SOC and SOC band gap calculations.

Material			Band gap (eV)	
A^+	M^{II}	M^{III}	Indirect	Direct
Cs	Sb	Cr	2.784	2.874
		Fe	3.551	3.552
		Cd	3.237	3.404
Rb		Cr	2.725	2.788
		Mn	-	3.512
		Cu	1.742	1.774
			Band gap (eV)	
			Non-SOC	SOC
Cs	Bi	Fe	3.824	3.327
		Mn	4.114	3.455
		Cd	3.958	3.636

Experimental Procedures

Material synthesis

General Considerations

Reagents were purchased from commercial vendors and used as received. Solvents were of reagent grade or higher purity. Methanol was HPLC quality and dried and degassed using a JC Meyer Solvent Purification system.

- **$Cs_4CdSb_2Cl_{12}$** was precipitated by adding 0.337 g of CsCl (2.0 mmol) to a solution of Sb_2O_3 (0.146 g, 0.5 mmol) and $CdCl_2$ (0.092 g, 0.5 mmol) in 2.5 mL of 36% HCl.

- **$Cs_4CdBi_2Cl_{12}$** was precipitated by adding 0.337 g of CsCl (2.0 mmol) to a solution of $BiCl_3$ (0.315 g, 1.0 mmol) and $CdCl_2$ (0.092 g, 0.5 mmol) in 2.5 mL of 36% HCl.

- **$Cs_4MnBi_2Cl_{12}$** was precipitated by adding 0.337 g of CsCl (2.0 mmol) to a solution of $BiCl_3$ (0.315 g, 1.0 mmol) and $MnCl_2$ (0.064 g, 0.5 mmol) in 2.5 mL of 36% HCl.

The precipitates were left under constant stirring for 12 hours. Then, they were thoroughly washed with diethyl ether three times to ensure that no HCl residue is left. Finally, they were dried at 120 ºC for 5 hours. Cadmium compounds: $Cs_4CdSb_2Cl_{12}$ and $Cs_4CdBi_2Cl_{12}$; were obtained as white microcrystalline powders, respectively; whereas $Cs_4MnBi_2Cl_{12}$ was obtained as a pale pink microcrystalline powder.

The Rb compounds were synthesized according to the following procedures:

- **$Rb_4CuSb_2Cl_{12}$** Inside a nitrogen-filled glovebox, a 5 mL methanolic solution containing 48.4 mg (0.1 mmol) of RbCl, was mixed with a 0.5 mL of solution containing 45.6 mg (0.2 mmol) of $SbCl_3$ and 13.4 mg of $CuCl_2$ (0.1 mmol) in anhydrous methanol. The resulting solution was then evaporated to dryness at 80 °C outside the glovebox, making sure that all volatiles were removed. A black, microcrystalline precipitate was obtained upon complete evaporation of the volatiles.

- **$Rb_4MnSb_2Cl_{12}$** was obtained by adding a 5 mL methanol solution with 48.4 mg (0.1 mmol) of RbCl, into a 0.5 mL methanol solution with 45.6 mg (0.2 mmol) of $SbCl_3$ and 12.6 mg of $MnCl_2$ (0.1 mmol). The resulting solution was then evaporated to dryness at 80 °C outside the glovebox, making sure that all volatiles were removed. A white-light pink precipitate forms after complete evaporation of the volatiles.

Material characterization

PXRD measurements

Powder X-Ray diffraction measurements were performed on a Bruker D8 Advance diffractometer with Cu K_α radiation (λ=1.54 Å) at 30 kV and 30 mA. The instrument was operating in a Bragg-Brentano geometry with a step increment of 0.02° and an acquisition time of one second per step.

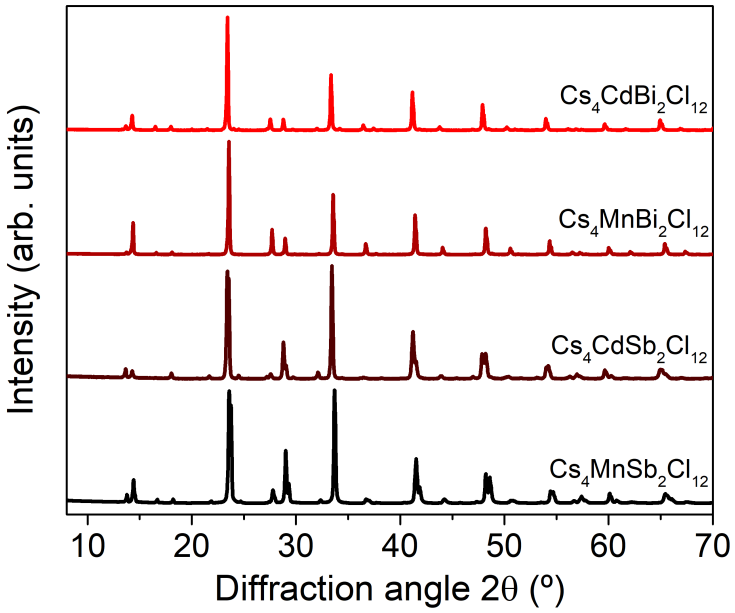

Figure S3. XRD patterns of the three new Cs-containing compounds compared with the $Cs_4MnSb_2Cl_{12}$ perovskite.

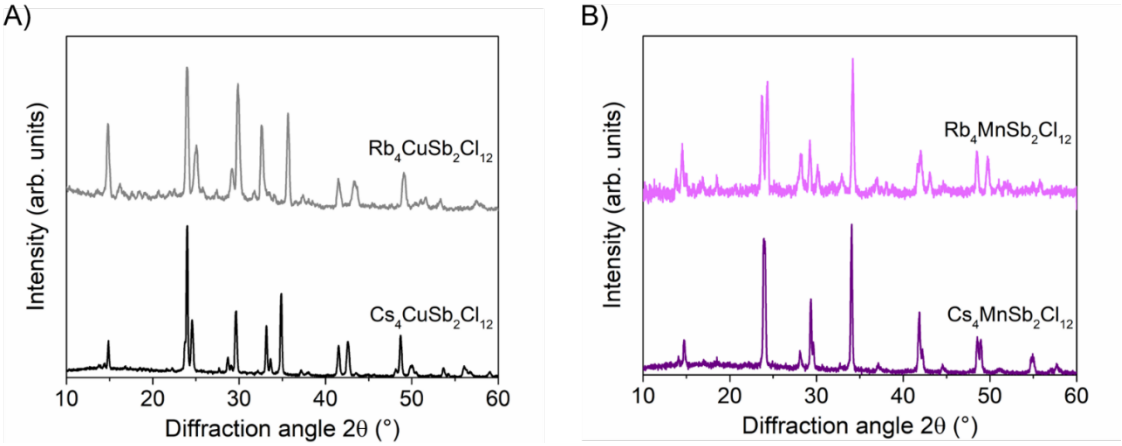

Figure S4. XRD patterns of A) the $A_4CuSb_2Cl_{12}$ (A = Rb and Cs) and B) $A_4MnSb_2Cl_{12}$ (A = Rb and Cs) perovskites.

Rietveld and Le Bail refinement

For XRD, the samples were ground in an agate mortar and the loose powder was pressed into a diffractometer sample holder. X-ray powder diffraction patterns were collected in Bragg-Brentano geometry at room temperature with CuK_α radiation (λ=1.54183 Å) in an Ultima IV diffractometer (from Rigaku) equipped with a D/tex detector. The sample patterns were recorded from 5 to 100° (2θ) in 0.02° steps and a scanning speed of 2°/min.

The structural refinement from XRD powder patterns was performed by the Rietveld method using the FULLPROF program.[12] The cell parameters and peak profiles were refined using the Le Bail pattern fitting method with pseudo-Voigt peak shape functions.[10] The background was modelled by a third-order polynomial fitting.

According to the XRD powder patterns, the synthesized samples of $Cs_4CdBi_2Cl_{12}$ and $Cs_4CdSb_2Cl_{12}$ was found to be hexagonal $R\bar{3}m$, a result in accordance to the structure obtained by single crystal.[13] The structure of these compounds was refined using the corresponding structural model obtained for single crystal. The final refinement, using the Rietveld method, was carried out on all atomic parameters while keeping the same values for the thermal parameters. Restrictions were also applied to interatomic distances.

The relevant crystallographic parameters; atomic positions (refined), thermal (B_{iso}) and occupation (Occ) factors as well as bond distances and angles of the compounds are compiled in Table S6, S7, and S8 respectively. The XRD powder patterns (experimental and calculated) of the samples are shown in Figure S5.

The Rb-compounds suffer from some degradation when exposed to X-ray radiation, so the structural refinement by the Rietveld method was no possible on these samples. Instead, the cell parameters and peak profiles were modelled using the Le Bail pattern fitting method[13] using a monoclinic C2/m space group. The Le Bail fitting was also attempted with the $R\bar{3}m$ trigonal space group, but the adjustment significantly improves with the monoclinic cell. The results are compiled in Table S9 and Figure S6.

Table S6. Experimental details for the XRD data recording and processing

	$Cs_4CdBi_2Cl_{12}$	$Cs_4CdSb_2Cl_{12}$	$Cs_4MnBi_2Cl_{12}$
Data collection			
Diffractometer	Rigaku, Ultima IV		
Detector	D/tex		
Wavelength (Å)	CuKα, 1.54183		
2θ range (°)	4-90	4-90	4-90
Step size (°)	0.02	0.02	0.02
scanning speed (°/min)	2	2	2
Indexing			
	M(18)= 51	M(20)= 27	M(20)=33
Unit cell			
Space Group	$R\bar{3}m$	$R\bar{3}m$	$R\bar{3}m$
Cell Parameters	a=b= 7.5903(2)	a=b= 7.5930(1)	a=b= 7.5446(1)
	c = 37.1638(14)	c = 36.8442(11)	c = 36.9099(11)
V(Å^3)	1854.25(10)	1839.61(8)	1819.47(7)
Z	3	3	3
Refinement			
# of reflections	223	221	216
# of refined parameters			
Structural	11	11	11
Profile	11	11	11
R_{exp}	2.45	2.35	2.54
R_{wp}	8.45	7.75	8.08
R_B	6.54	5.69	5.96
S	3.44	3.30	3.18

Table S7. Refined atomic positions, thermal (B_{iso}) and occupation (Occ) factors for the materials under study.

Composition	site	x	y	z	Biso	Occ
$Cs_4Bi_2CdCl_{12}$						
Cs1	6c	2/3	1/3	0.4597(3)	1.58(4)	1
Cs2	6c	0	0	0.6231(3)	1.58(4)	1
Bi	6c	2/3	1/3	0.5873(1)	1.27(3)	1
Cd	3b	0	0	1/2	2.0(1)	1
Cl1	18h	0.8397(9)	0.1603(9)	0.5394(4)	2.6(3)	1
Cl2	18h	0.5085(7)	0.4915(7)	0.6287(4)	2.6(3)	1
$Cs_4Sb_2CdCl_{12}$						
Cs1	6c	2/3	1/3	0.4604(1)	1.01(2)	1
Cs2	6c	0	0	0.6231(1)	1.01(2)	1
Sb	6c	2/3	1/3	0.5879(1)	0.8(2)	1
Cd	3b	0	0	1/2	1.37(2)	1
Cl1	18h	0.8405(6)	0.1595(6)	0.5444(3)	1.683)	1
Cl2	18h	0.5053(6)	0.4947(6)	0.6289(2)	1.683)	1
$Cs_4Bi_2MnCl_{12}$						
Cs1	6c	2/3	1/3	0.4585(1)	1.64(2)	1
Cs2	6c	0	0	0.6231(1)	1.64(2)	1
Bi	6c	2/3	1/3	0.5868(1)	1.33(2)	1
Mn	3b	0	0	1/2	2.3(2)	1
Cl1	18h	0.8394(6)	0.1606(6)	0.5374(3)	2.1(3)	1
Cl2	18h	0.5071(6)	0.4929(6)	0.6294(2)	2.1(3)	1

Table S8. Bond distances (in Å) and angles (°) from the refined structures: $Cs_4Bi_2CdCl_{12}$, $Cs_4Sb_2CdCl_{12}$ and $Cs_4Bi_2MnCl_{12}$.

$Cs_4Bi_2CdCl_{12}$	
Bond distance (Å)	Angle (°)
Cd-Cl1=2.568(2)	Cl2-Bi-Cl2= 88.29(2)
Bi-Cl1=2.511(2)	Cl2-Bi-Cl1= 92.87(1)
Bi-Cl2=2.897(2)	Cl2-Bi-Cl1= 178.38(2)
	Cl1-Bi-Cl1= 85.95(2)
	Cl1-Cd-Cl1= 89.27(2)
	Cl1-Cd-Cl1= 90.72(2)
	Cl1-Cd-Cl1= 180.0
	Cd-Cl1-Bi= 176.67(2)

$Cs_4Sb_2CdCl_{12}$	
Bond distance (Å)	Angle (°)
Cd-Cl1=2.662(2)	Cl2-Sb-Cl2= 89.85(2)
Sb-Cl1=2.606(2)	Cl2-Sb-Cl1= 89.87(1)
Sb-Cl2=2.794(2)	Cl2-Sb-Cl1= 179.61(2)
	Cl1-Sb-Cl1= 90.40(2)
	Cl1-Cd-Cl1= 86.18(2)
	Cl1-Cd-Cl1= 93.82(2)
	Cl1-Cd-Cl1= 180.0
	Cd-Cl1-Sb= 177.06(2)

$Cs_4Bi_2MnCl_{12}$	
Bond distance (Å)	Angle (°)
Mn-Cl1=2.512(2)	Cl2-Bi-Cl2= 87.56(2)
Bi-Cl1=2.903(2)	Cl2-Bi-Cl1= 93.87(1)
Bi-Cl2=2.609(2)	Cl2-Bi-Cl1= 178.01(2)
	Cl1-Bi-Cl1= 84.67(2)
	Cl1-Mn-Cl1= 87.31(2)
	Cl1-Mn-Cl1= 92.69(2)
	Cl1-Mn-Cl1= 180.0
	Cd-Cl1-Bi= 174.38(2)

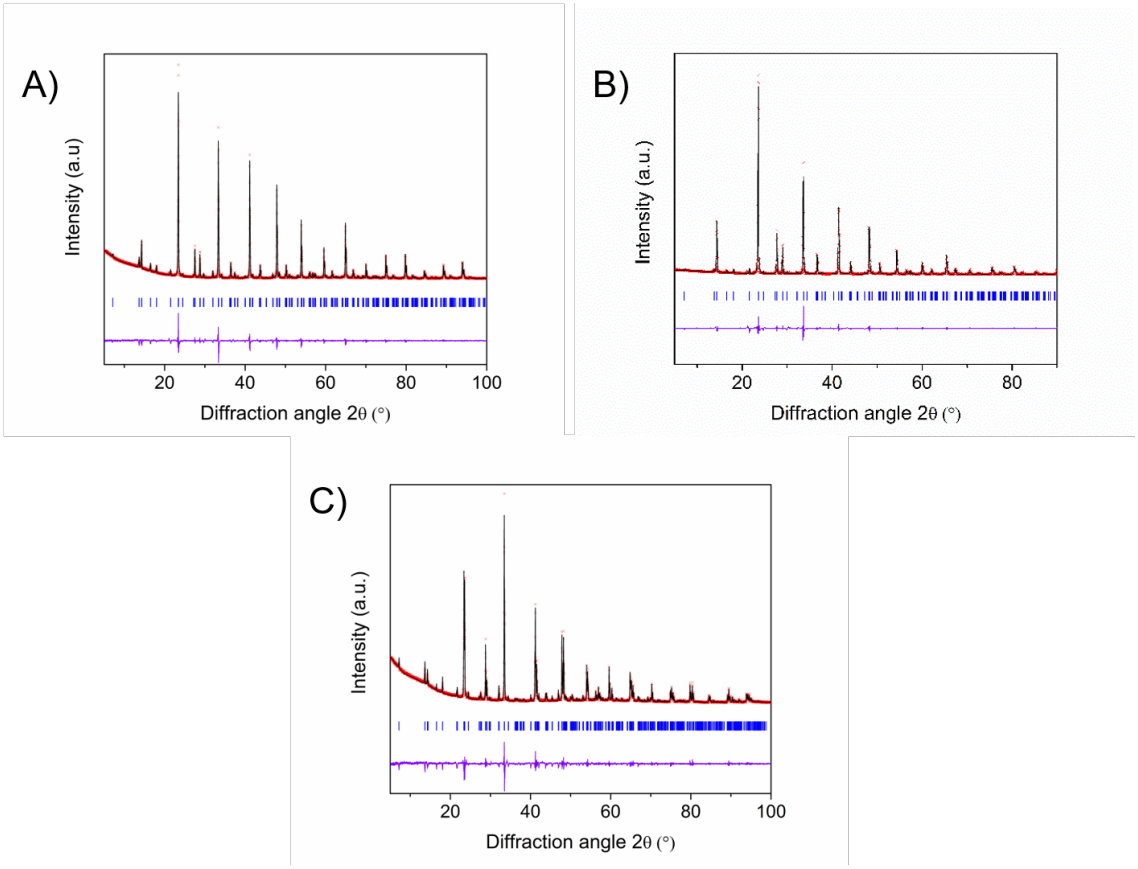

Figure S5. Observed (black line), calculated (crosses) and differences profiles (lower trace) for the Rietveld refinement for A) $Cs_4CdSb_2Cl_{12}$, B) $Cs_4CdBi_2Cl_{12}$ and C) $Cs_4MnBi_2Cl_{12}$.

Table S9. Cell parameters of the Rb-materials obtained from the *Le Bail* refinement.

	$Rb_4CuSb_2Cl_{12}$	**$Rb_4MnSb_2Cl_{12}$**
Unit cell		
Space Group	*C*2/*m*	*C*2/*m*
Cell Parameters	a=13.161	a=13.127
	b=7.400	b=7.359
	c=12.872	c=12.996
	β=111.65	β=111.57

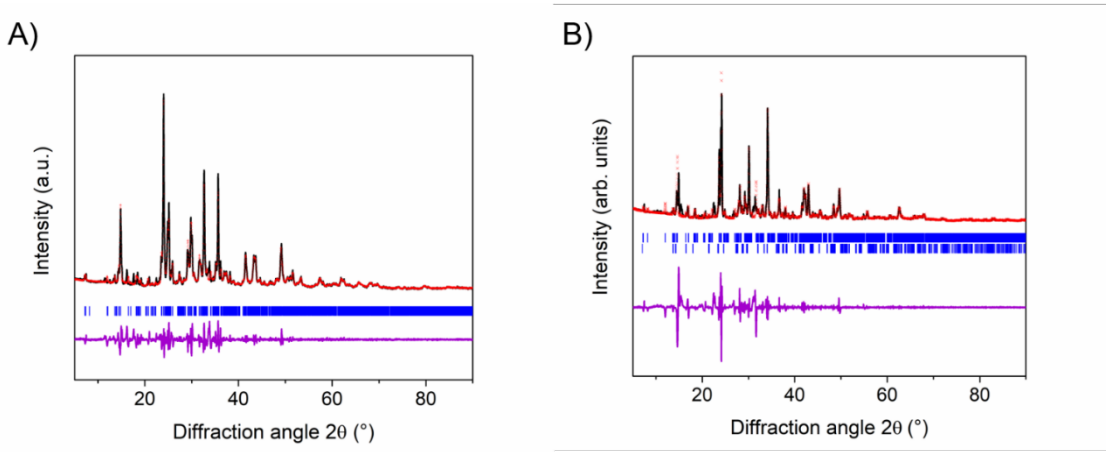

Figure S6. Observed (black line), calculated (crosses) and differences profiles (lower trace) for the Rietveld refinement for A) $Rb_4CuSb_2Cl_{12}$ and B) $Rb_4MnSb_2Cl_{12}$.

Thermogravimetric and differential scanning results

Thermogravimetric analysis was performed with a TGA Q5000 V3.17 Build 265 (TA Instruments) in nitrogen (flow rate 10 mL/min) with a platinum pan at a heating rate of 10 °C/min. The temperature range was from 30 °C to 500 ºC for $Cs_4CdSb_2Cl_{12}$, from 30 °C to 700 ºC for $Cs4CdBi_2Cl_{12}$ and $Cs_4MnBi_2Cl_{12}$ and from 30 °C to 300 °C for $Rb_4CuSb_2Cl_{12}$ and $Rb_4MnSb_2Cl_{12}$. Differential thermal analysis was performed with a DSC Q2000 V24.11 Build 124 (TA Instruments) in a nitrogen atmosphere (flow rate 50 mL/min) with aluminum pan at a heating rate of 10 °C/min. The temperature range was from –85 °C to 300 °C for all samples.

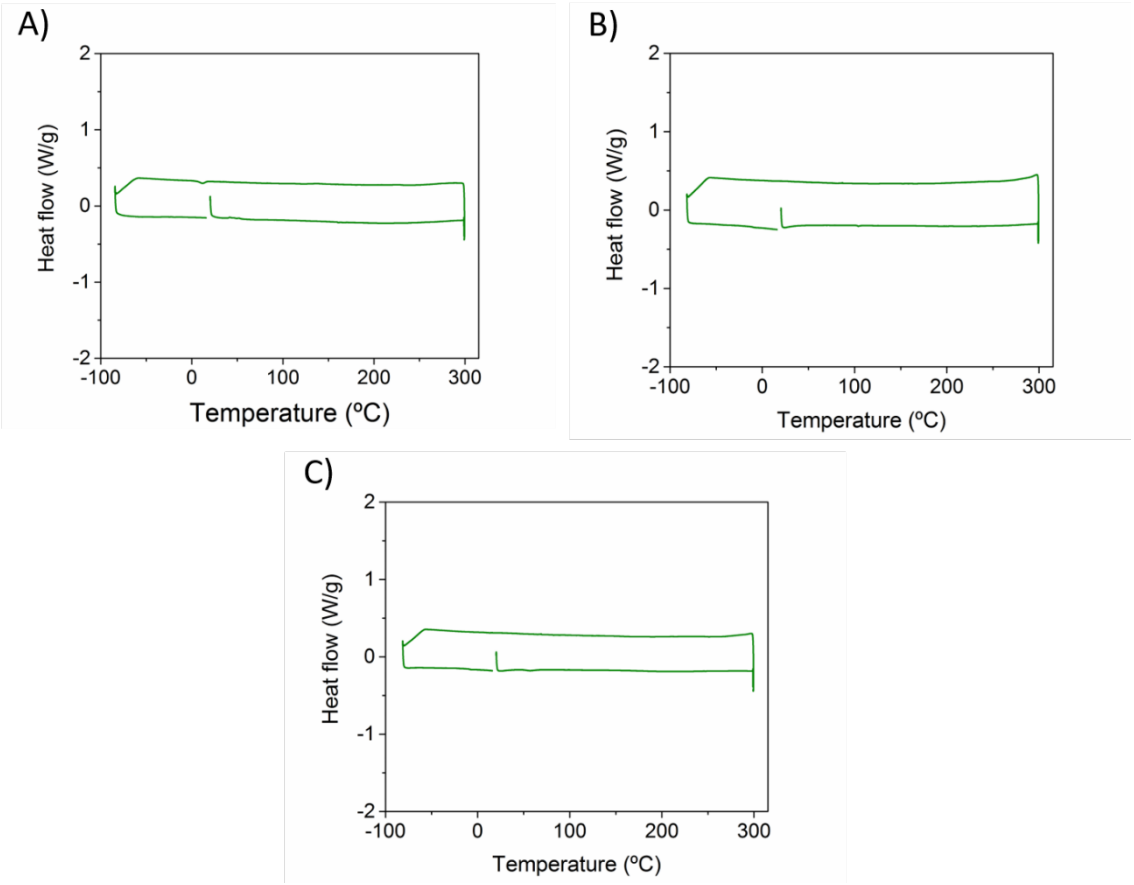

Figure S7. Differential scanning calorimetry of A) $Cs_4CdSb_2Cl_{12}$, B) $Cs_4CdBi_2Cl_{12}$ and C) $Cs_4MnBi_2Cl_{12}$.

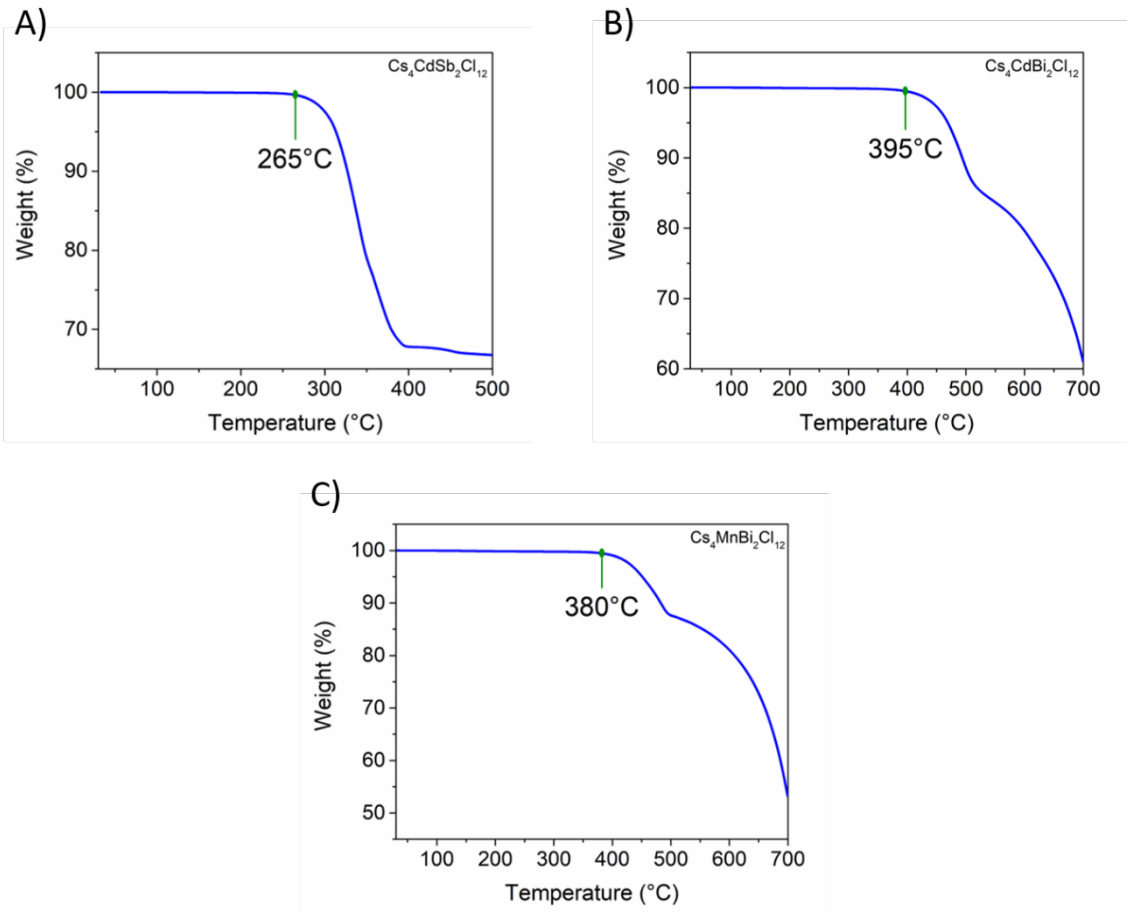

Figure S8. Thermogravimetric analysis of A) $Cs_4CdSb_2Cl_{12}$, B) $Cs_4CdBi_2Cl_{12}$ and C) $Cs_4MnBi_2Cl_{12}$.

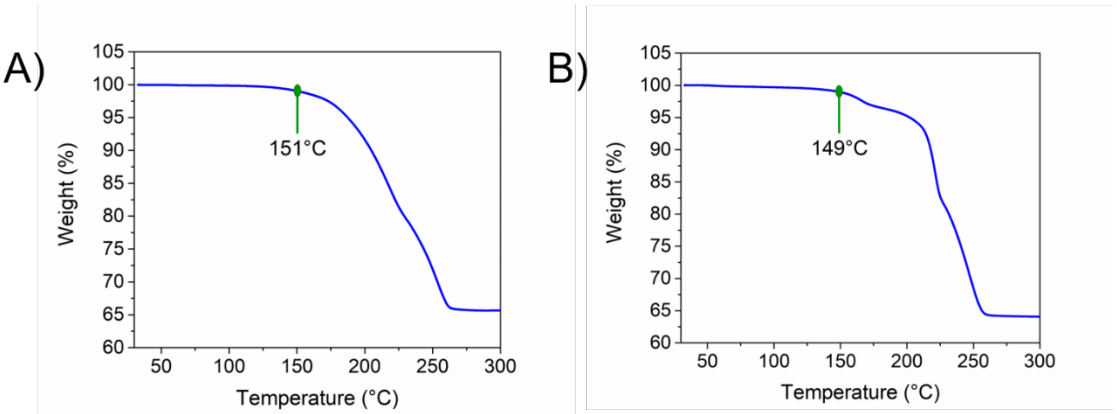

Figure S9. Thermogravimetric analysis of A) $Rb_4CuSb_2Cl_{12}$ and B) $Rb_4MnSb_2Cl_{12}$.

Stability towards humidity and light

The Cs-materials stability XRD measurements were performed on a D5000 Siemens diffractometer with Co K_α radiation (λ=1.79 Å) at 34 kV and 30 mA. The instrument was operating in a Bragg Brentano geometry with a step increment of 0.02° and an acquisition time of 0.6 s per step.

The Rb-materials stability XRD measurements were performed on an Ultima IV Rigaku diffractometer with Cu K_α radiation (λ=1.54183 Å) working at 40 kV and 44 mA. The instrument was operating in a Bragg Brentano geometry with a step increment of 0.02° and an acquisition time of 1.6° per minute.

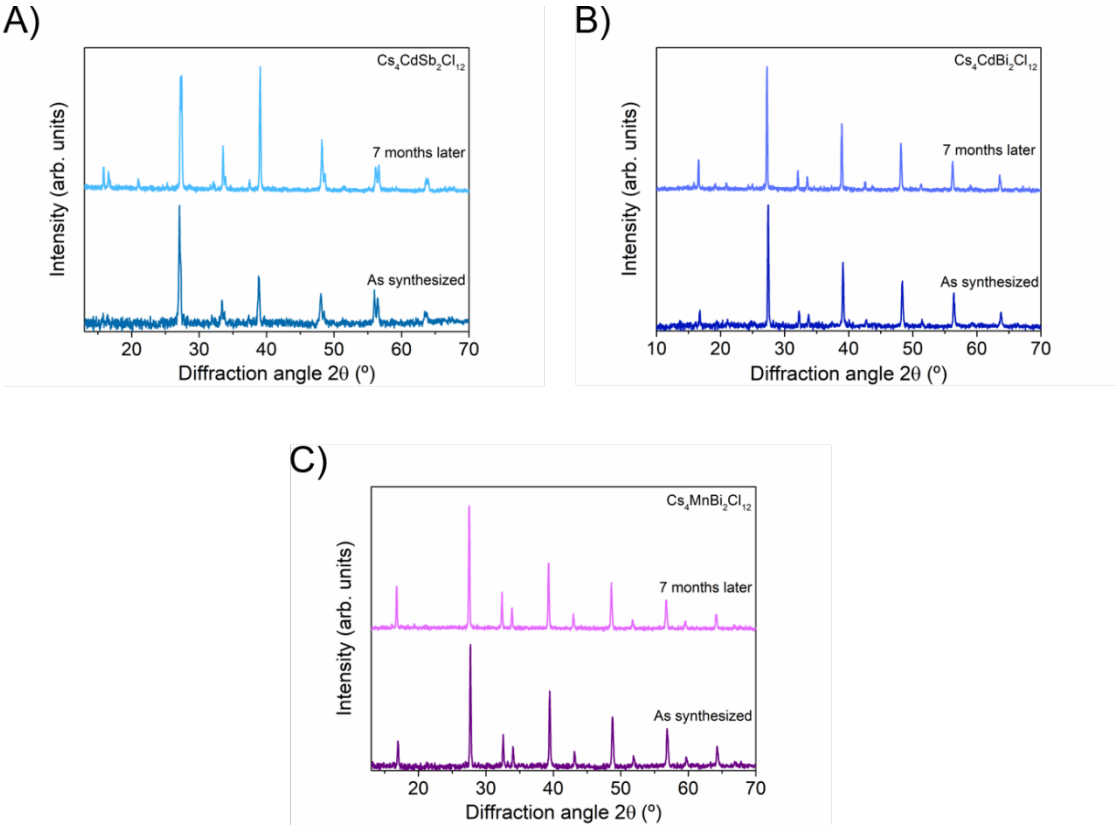

Figure S10. XRD patterns of A) $Cs_4CdSb_2Cl_{12}$, B) $Cs_4CdBi_2Cl_{12}$ and C) $Cs_4MnBi_2Cl_{12}$ after 7 months exposure to moisture and heat.

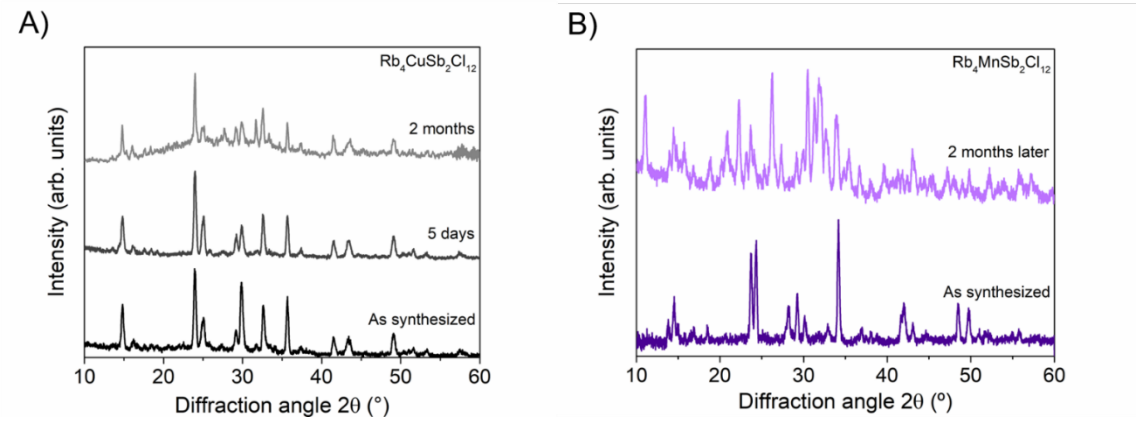

Figure S11. XRD patterns of A) $Rb_4CuSb_2Cl_{12}$ and B) $Rb_4MnSb_2Cl_{12}$ after 2 months exposure to moisture and heat.

Photoluminescence and absorbance measurements

Excitation and emission photoluminescence spectra were recorded with a Horiba Fluoromax-4 spectrofluorometer using a 400 nm low-pass filter and the appropriate bandpass filter depending on the sample.

Absorption measurements were recorded using a Shimadzu spectrophotometer UV-2600 equipped with an ISR-2600 Plus integrated sphere and collected using absorbance data on a bulk powder sample. A $BaSO_4$ blank was used for the measurements.

Band gaps were extracted by fitting the linear regions of a plot of $(\alpha * h\nu)^2$ vs *E and* $(\alpha * h\nu)^{1/2}$ vs E (where E = photon energy) and determining the *x*-intercept.

Table S10. Calculated direct and indirect band gaps of the synthesized materials.

Material	Direct (eV)	Indirect (eV)
$Cs_4CdBi_2Cl_{12}$	3.2	2.9
$Cs_4MnBi_2Cl_{12}$	3.1	2.8
$Cs_4CdSb_2Cl_{12}$	3.0	2.7
$Rb_4CuSb_2Cl_{12}$	0.9	0.6
$Rb_4MnSb_2Cl_{12}$	3.2	2.9

References

[1] P. E. Blöchl, *Phys. Rev. B* **1994**, *50*, 17953–17979.

[2] G. Kresse, J. Hafner, *Phys. Rev. B* **1993**, *47*, 558–561.

[3] G. Kresse, J. Furthmüller, *Comput. Mater. Sci.* **1996**, *6*, 15–50.

[4] J. P. Perdew, A. Ruzsinszky, G. I. Csonka, O. A. Vydrov, G. E. Scuseria, L. A. Constantin, X. Zhou, K. Burke, *Phys. Rev. Lett.* **2008**, *100*, 136406.

[5] Y. Hinuma, G. Pizzi, Y. Kumagai, F. Oba, I. Tanaka, *Comput. Mater. Sci.* **2017**, *128*, 140–184.

[6] B. Vargas, E. Ramos, E. Pérez-Gutiérrez, J. C. Alonso, D. Solis-Ibarra, *J. Am. Chem. Soc.* **2017**, *139*, 9116–9119.

[7] B. Vargas, R. Torres-Cadena, J. Rodríguez-Hernández, M. Gembicky, H. Xie, J. Jiménez-Mier, Y.-S. Liu, E. Menéndez-Proupin, K. R. Dunbar, N. Lopez, et al., *Chem. Mater.* **2018**, *30*, 5315–5321.

[8] A. Jain, S. P. Ong, G. Hautier, W. Chen, W. D. Richards, S. Dacek, S. Cholia, D. Gunter, D. Skinner, G. Ceder, et al., *APL Mater.* **2013**, *1*, 011002.

[9] Heyd, J., Scuseria, G. E., & Ernzerhof, M. *J. Chem. Phys.* **2003**, *118*, 8207–8215.

[10] Heyd, J., Scuseria, G. E., & Ernzerhof, M. *J. Chem. Phys.* **2006**, *124*, 219906.

[11] Wang, X.; Meng, W.; Xiao, Z.; Wang, J.; Mitzi, D.; Yan, Y. **2017**, arXiv:1707.09539 [cond-mat.mtrl-sci]. arXiv.org e-Print archive. https://arxiv.org/abs/1707.09539.

[12] Rodríguez-Carvajal, J*. Physica B Condens Matter.* **1993**, *192*, 55-69.

[13] Le Bail, A. *Powder Diffr.* **2005**, *20*, 316-326.